

Polymeric filament thinning and breakup in microchannels

P.E. Arratia¹, J.P. Gollub^{1,2}, and D.J. Durian¹

¹*Department of Physics and Astronomy, University of Pennsylvania, Philadelphia, PA 19104*

²*Department of Physics, Haverford College, Haverford, PA 19041*

(Dated: May 26, 2019)

The effects of elasticity on filament thinning and breakup are investigated in microchannel cross flow. When a viscous solution is stretched by an external immiscible fluid, a low 100 ppm polymer concentration strongly affects the breakup process, compared to the Newtonian case. At late times when viscoelastic stresses become important, polymer filaments show much slower evolution, morphology featuring multiple connected drops, and different scaling with the ratio of flow rates. The filament thinning process can be described in terms of extensional viscosities of the immiscible fluids, which for the polymer solution includes strain hardening.

PACS numbers: 47.50.+d, 83.60.Wc, 05.45-a, 83.50 -v

The progressive breakup of an initially stable fluid thread into small drops or bubbles is a rich phenomenon of great interest [1]. For example, flow focussing in microfluidic devices can continuously produce drops or bubbles whose sizes are controlled by the relative flow rate of the two immiscible fluids [2, 3, 4, 5, 6, 7]. While most such work concerns Newtonian fluids, many fluids of interest for lab-on-a-chip applications are likely to exhibit complex micro-structure and non-Newtonian behavior, such as viscoelasticity. Furthermore, viscoelastic effects scale inversely with the square of the device length scale, and hence are likely to be accentuated in microfluidic devices. For polymeric drop breakup in macroscopic flow, elasticity can give rise to breakup behavior that is markedly different from that of Newtonian fluids [8, 9, 10, 11]. For example, a viscoelastic filament driven by gravity in a quiescent bath [12] undergoes an initial linear viscous decrease in the filament diameter, followed by a slower thinning process in which capillary forces are balanced by the fluid elastic stresses.

Recently, a numerical investigation in a flow-focusing device [13] showed qualitative differences with respect to Newtonian fluids such as prolonged thinning of the fluid filament and delay of drop pinch-off. No measurements of thinning rates or breakup times were presented. An experimental investigation in a ‘T’ shaped geometry using a low viscosity, elastic fluid [14] also found prolonged thinning of the fluid filament. The authors observed a linear decrease in filament diameter followed by a ‘self-thinning’ exponential regime, which was argued to have a rate inversely proportional to the fluid relaxation time (λ). However, λ was found to vary over an order of magnitude with shear rate, though it should remain constant; the authors associated this discrepancy with ‘pre-shearing’ effects. While both investigations found similar qualitative trends, no quantitative connection has yet been made to the extensional flow within the filament during thinning and breakup.

In this paper, we compare the filament thinning and breakup of Newtonian and viscoelastic fluids of equal

shear viscosity in a microchannel cross geometry. Here the outer Newtonian fluid shears and stretches the inner Newtonian or polymeric fluid into a thin filament until it eventually breaks up into drops. This geometry allows for very fine control of the flows over a broad range of shear rates, while the choice of fluids emphasizes the role of extensional viscosity in the thinning behavior. The latter allows comparison with a microscopic model relating polymer extension to rheology.

The experimental configuration is a cross slot microchannel, $W = 50 \mu\text{m}$ wide and $L = 30 \mu\text{m}$ deep, molded in poly(dimethylsiloxane) (PDMS, Dow Sylgard 184) using standard soft-lithography methods [15, 16]. Channels are sealed with a glass cover slip after exposure to an oxygen plasma. In order to keep the microchannel wetting properties uniform, the glass cover slip is coated with a thin layer of PDMS prior to the exposure. The assembled channels are then baked for 12 hrs at 100 °C in order to obtain hydrophobic walls wetted by the continuous liquid phase.

The continuous phase is mineral oil containing 0.1% by weight of surfactant (SPAN. 80). Two types of dispersed phases are used: a Newtonian fluid and a polymeric fluid. The Newtonian fluid is a 90%-glycerin aqueous solution. The polymeric fluid is made by adding 100 ppm of high molecular weight polyacrylamide (PAA, $M_W = 18 \times 10^6$, 15% polydispersity), which has a flexible backbone, to an 85%-glycerin aqueous solution. It is dilute, well below the overlap concentration of approximately 350 ppm. The interfacial tension between the continuous and dispersed phases is $\sigma = 10 \text{ mN/m}$. Shear rheology is characterized with a stress-controlled rheometer at 25 °C. As shown in Fig. 1, the shear viscosities of the oil and Newtonian fluids are nearly identical and independent of shear rate: $\eta_s \approx 0.24 \text{ Pa s}$. Also as shown, the viscoelastic polymeric fluid exhibits a first normal stress difference, N_1 , which increases with shear rate. We fit η_s and N_1 data to the widely-used FENE-P (finite extensibility nonlinear elastic) model, in which the polymer molecules are represented as dumb-bells that can be stretched by a finite

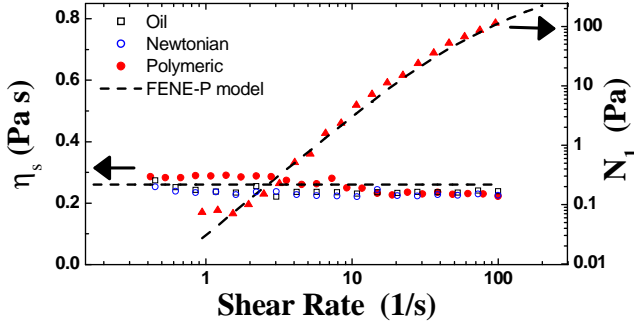


FIG. 1: (Color Online) Fluid rheological characterization. (Left y-axis) Shear viscosity vs shear rate for all fluids; oil=mineral oil; Newtonian=water/glycerin mixture; polymeric=PAA in water/glycerin mixture. The shear viscosity is nearly constant even for the polymer solution $\eta_s \approx 0.24$ Pa s. (Right y-axis) First normal stress difference for the polymeric solution vs shear rate. Dashed curves represent fits using the FENE-P model with parameters $\lambda = 0.45$ s and $b = 4500$.

amount in the flow field [17, 18]. The fit provides the fluid relaxation time λ and a dimensionless finite extensibility parameter b .

The dispersed and continuous phases are injected into the central and side arms of the cross-channel, respectively, using syringe pumps (Harvard Instruments). Experiments are performed for flow rate ratios, $q = Q_{oil}/Q_{aq}$, ranging from 10 to 200. In all cases, the aqueous flow rate is kept constant at $Q_{aq} = 0.01$ $\mu\text{l}/\text{min}$. This is low enough that the behavior is quasi-static, such that the periodicity -but not the morphology- depends Q_{aq} . For this range of parameters, the Reynolds number is less than 0.01; therefore viscous forces are much larger than inertial forces. Similarly the capillary number ranges from 0.02 to 0.8; therefore, viscous forces are also larger than surface forces. Under these conditions an aqueous filament is formed and stretched by the flow of the surrounding oil. The thinning and breakup of the filament are imaged using an inverted microscope and a fast video camera, with frame rates between 1 and 10 kHz.

Example stills from video data are shown in Fig. 2, for both Newtonian and polymeric fluids, at a flow rate ratio of $q = 60$. The Newtonian case, shown in the *left-column*, displays typical filament thinning and drop formation. The aqueous phase is drawn into the cross-slot channel (a), and begins to elongate and collapse (b-d), forming a primary drop connected by a very thin filament; later (e) the filament thins at a faster rate and breaks into a large primary drop and small satellite droplets.

The polymeric case, shown in the *right-column* of Fig. 2, displays very different behavior. Initially (a), we observe a morphology that is similar to that of the Newtonian fluid, i.e. viscoelasticity is negligible at first. As the thinning progresses, the polymeric fluid develops a longer neck with a drop attached to it (b). This filament elongates while thinning at a slower rate than in the New-

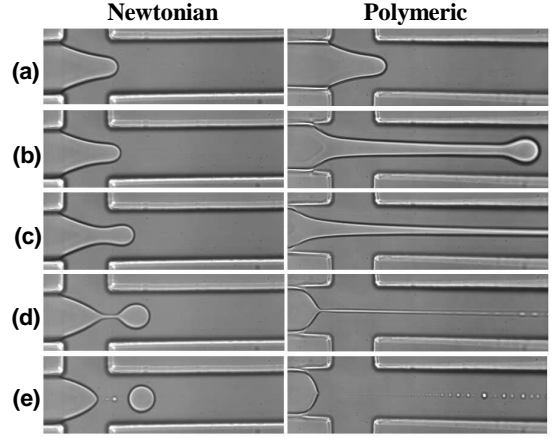


FIG. 2: Evolution of the thinning process for Newtonian (left column) and polymeric fluids (right column), for a flow rate ratio $q = Q_{oil}/Q_{aq} = 60$, where Q_{oil}/Q_{aq} corresponds to the oil and aqueous phase flow rates, respectively. Oil is the continuous (outer) phase while the aqueous phase is either Newtonian or polymeric. (a) Initial regime; (b) $t/t_b = 0.15$, where t_b is breakup time; (c) $t/t_b = 0.45$; (d) $t/t_b = 0.95$; (e) after breakup. Values of t_b for the Newtonian and polymeric cases are 11.5 ms and 245 ms, respectively. Note the appearance of satellite droplets in the Newtonian case and multiple beads attached to the filament in the polymeric case (d,e). The channel width and depth are 50 μm and 30 μm , respectively.

tonian case (c). Near the breakup event, the polymeric fluid shows multiple beads ('beads-on-a-string') attached to the filament (d) [8, 10, 19]. After breakup, there are many satellite drops (e).

Filament thinning may be quantified by the decrease in diameter, $h(t)$, as a function of time. To accomplish this, we first fit a third-order polynomial equation to the interface contour in the cross slot region. We then locate the minimum in the polynomial first derivative, and measure the filament diameter at this point. Example results are shown in Fig. 3(a) for three flow rate ratios, $q = 10, 30$, and 60. At short times, the Newtonian and polymeric fluids exhibit identical initial thinning, which is indicative of their common shear viscosity. But at longer times, the two diverge with the polymeric filament lasting at least an order of magnitude longer before breakup.

The filament strain rate may be computed from $h(t)$ data by assuming a homogeneous uniaxial flow inside the filament with extensional strain rate equal to $\dot{\epsilon} = -(2/h)dh/dt$ [20, 21]. Results for the same three flow rate ratios are given in Fig. 3(b). For the Newtonian fluid, $\dot{\epsilon}$ is initially independent of time; therefore, in this regime, $h(t)$ decreases exponentially with time. For the polymeric fluid, $\dot{\epsilon}$ is initially equal to the same constant as for the Newtonian fluid. But it soon departs and, after a transient interval, settles down to smaller constant value, indicating a second regime of slower exponential thinning. For all fluids at the very latest times, close to breakup, the final decrease of $h(t)$ to zero gives an appar-

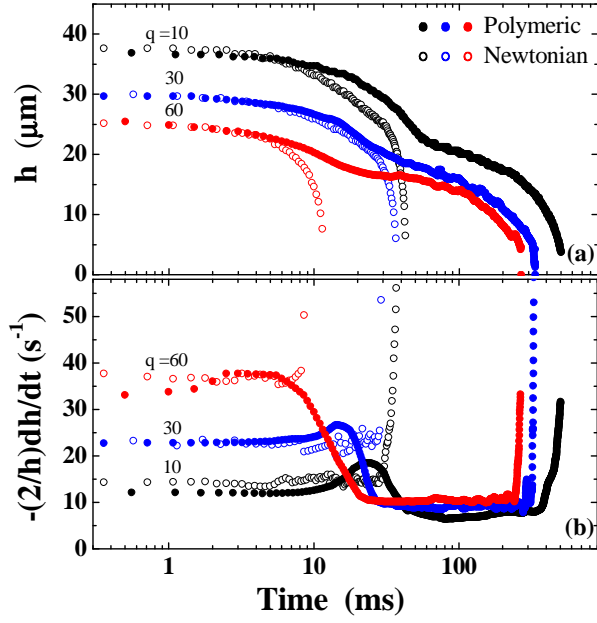


FIG. 3: (Color Online) (a) Filament thickness $h(t)$ for both Newtonian and polymeric fluids for flow rate ratios $q=10$, 30, and 60. (b) Filament extensional strain rate $\dot{\epsilon}=-(2/h)dh/dt$ for the same fluids. Both viscous and elastic regimes are characterized by constant $\dot{\epsilon}$.

ent divergence of $\dot{\epsilon}$. We show in the following discussion that the data just before breakup are consistent with a linear decrease in filament diameter, $h(t) \propto (t - t_b)$ where t_b is the breakup time.

To model the exponential decrease of filament diameter, we start from an expression of stress balance $\eta_e \dot{\epsilon} = \eta_{e,oil} \dot{\epsilon}_{oil}$, where left and right hand sides are extensional viscosity times extensional strain rate for the aqueous filament and continuous oil phases, respectively. As noted above, the strain rate in the filament is $\dot{\epsilon} = -(2/h)dh/dt$. The strain rate for oil in the cross-slot region is $\dot{\epsilon}_{oil} \approx Q_{oil}/(W^2L)$, as verified by particle-tracking methods [22]. And lastly, since the oil is Newtonian, its extensional viscosity is $\eta_{e,oil} = 3\eta_{s,oil}$ [23, 24]. Therefore, also assuming that η_e is independent of time, the filament diameter thins exponentially according to

$$h(t) = h_o \exp[-(3/2)(\eta_{s,oil}/\eta_e)\dot{\epsilon}_{oil}t]. \quad (1)$$

where h_o is an integration constant. In such *flow-driven* regimes, Eq. (1) may be used to deduce η_e from $h(t)$ data.

The linear decrease of the filament thickness near the final breakup can also be modeled by stress balance, now by incorporating surface tension effects. Specifically, the Rayleigh-Plateau instability eventually sets in so that capillary forces cause beading and ultimately breakup. Equating radial stress with the Laplace pressure gives $\eta_e \dot{\epsilon} = \sigma/h$ [7, 25, 26]. Therefore, the filament diameter thins linearly with time according to

$$h(t) = -(1/2)(\sigma/\eta_e)(t - t_b), \quad (2)$$

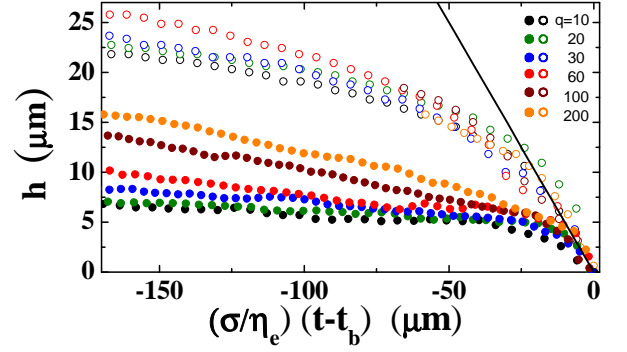


FIG. 4: (Color Online) Capillary driven breakup regime. At very late times, the filament thins roughly linearly in time with a speed proportional to σ/η_e for both Newtonian (open circles) and polymeric (filled circles) fluids. The flow ratio (q) is color-coded in the legend for both cases. The solid line represents slope $=-1/2$.

where t_b is the breakup time. In such *capillary-driven* regimes, Eq. (2) may be used to deduce η_e from $h(t)$ data.

To demonstrate the consistency of extensional viscosity results from the flow- and capillary-driven regimes, we plot data for $h(t)$ vs $(\sigma/\eta_e)(t - t_b)$ in Fig. 4. There, the value of η_e is taken from analysis of the flow-driven regime using Eq. (1). To within apparently random deviations, $h(t)$ data vanish linearly vs $(\sigma/\eta_e)(t - t_b)$ with slope $-1/2$, in accord with Eq. (2). Note however that the dynamic range is limited, since the imaging resolution is about $2 \mu\text{m}$. Therefore, the capillary-driven regime is consistent with the flow-controlled regime, but the latter gives more accurate values of η_e .

Final results for extensional viscosity, η_e , based on Eq. (1), are plotted in Fig. 5 vs extensional strain rate. Here each point represents a different fixed flow-rate ratio, q . For the Newtonian fluid, η_e is independent of strain rate and nearly equals $3\eta_s$ as expected [23, 24]. This agreement serves as a second check, complementary to Fig. 4. For the polymeric fluid early in the flow-driven regime, the behavior is the same as for the Newtonian fluid (not shown). Later in the flow-driven regime, the extensional strain rate of the filament is lower and η_e is higher. This behavior is due to the stretching of the polymer molecules in the extensional flow of the thinning filament.

The extensional properties of polymeric fluids are important for applications such as turbulent drag reduction and splash suppression [23, 27]; however, measurement of η_e has remained a difficult task [28]. Our method gives high-quality data, which may now be compared with existing predictions. The FENE-P model is the most widely-used. In Fig. 1, it well describes both the shear viscosity and the first normal stress difference vs shear rate with three adjustable parameters. Using these values, the FENE-P prediction for extensional viscosity

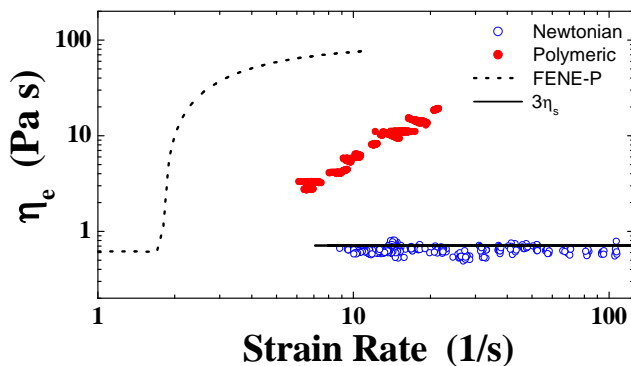


FIG. 5: (Color Online) Extensional viscosities of both Newtonian and polymeric fluids, derived from the filament thinning measurements and Eq. (1), as a function of the extensional strain rate $\dot{\epsilon} = -2/h(dh/dt)$. The polymeric fluid extensional viscosity shows strain hardening and increases with a power law exponent of approximately 1.0. The theoretical Trouton ratio of a Newtonian fluid is 3.0 (solid line). The FENE-P model prediction is also shown, but is far from the measurements.

is plotted in Fig. 5. It exhibits strain-hardening, which saturates at high strain rates by accounting for the finite extensibility of the polymer molecules. However, by comparison with our data, the predicted strain hardening sets in too soon and too abruptly. A possible cause for this discrepancy may be polymer dispersivity ($\sim 15\%$ in M_W), which can smear out the sharp rise in η_e [9]. It cannot, however, account for such early transition to strain hardening behavior since $\lambda \sim M_W^{3/2}$.

In conclusion, small amounts of flexible polymer can dramatically affect filament thinning and breakup in micro-channel extensional flow. In contrast to macroscopic observations, we find both a *flow-driven* regime in which the filament thins followed by a *capillary-driven* regime responsible for filament breakup. For a Newtonian fluid, the filament thins exponentially with time until onset of capillary surface tension-induced breakup. For a polymeric fluid, with the same shear viscosity - independent of shear rate, there is an intermediate regime in which the filament thins exponentially at a much slower rate. Furthermore the capillary regime features generation of a series of small droplets along the filament. These differences may be attributed solely to extensional viscosity, and its increase with extensional strain rate, since this is the only rheological difference between the Newtonian and polymeric fluids. For thinner filaments and faster thinning, the polymer molecules stretch and cause an increase in extensional viscosity without significant change in shear viscosity. Measurements of the exponential rate of thinning can thus be used to determine extensional viscosity, an elusive quantity to measure. For the Newtonian case, η_e is three times the shear viscosity; for the polymeric case, the results increase with exten-

sional strain rate but much less slowly than predicted by the widely-used FENE-P model. This suggests the need for a better understanding of both the molecule-scale behavior of polymers in extensional flows as well as its connection to macroscopic rheology. Filament thinning in microchannels, and its variations with polymer molecular weight, may be a promising approach.

We thank Daniel Bonn and Howard Stone for fruitful discussions as well as Seth Fraden and Katie Humphry for help with microfabrication methods. Kerstin Nordstrom and Ben Polak provided assistance with experiments. This work was supported the National Science Foundation through grant MRSEC/DMR05-20020.

-
- [1] J. Eggers, Rev. Mod. Phys. **69**, 865 (1997).
 - [2] S. Anna, N. Bontoux, and H. Stone, Appl. Phys. Lett. **82**, 364 (2003).
 - [3] R. Dreyfus, P. Tabeling, and H. Willaime, Phys. Rev. Lett. **90**, 144505 (2003).
 - [4] J. Gordillo *et al.*, Phys. Fluids **16**, 2828 (2004).
 - [5] P. Garstecki *et al.*, Appl. Phys. Lett. **85**, 2649 (2004).
 - [6] D. Link *et al.*, Phys. Rev. Lett. **92**, 054503 (2004).
 - [7] P. Garstecki, H. Stone, and G. Whitesides, Phys. Rev. Lett. **94**, 164501 (2005).
 - [8] M. Goldin *et al.*, J. Fluid Mech. **38**, 689 (1969).
 - [9] C. Wagner *et al.*, Phys. Rev. Lett. **95**, 164504 (2005).
 - [10] C. Clasen *et al.*, J. Fluid Mech. **556**, 283 (2006).
 - [11] V. Tirtaatmadja, G. McKinley, and J. Cooper-White, Phys. Fluids **18**, 043101 (2006).
 - [12] V. Entov and E. Hinch, J. Non-Newt. Fluid Mech. **72**, 31 (1997).
 - [13] C. Zhou, P. Yue, and J. Feng, Phys. Fluids **18**, 092105 (2006).
 - [14] J. Husny and J. Cooper-White, J. Non-Newt. Fluid Mech. **137**, 121 (2006).
 - [15] S. Quake and A. Scherer, Science **290**, 1536 (2000).
 - [16] S. Sia and G. Whitesides, Electroph. **24**, 3563 (2003).
 - [17] R. Bird, C. Curtiss, R. Armstrong, and O. Hassager, *Dynamics of Polymeric Liquids: Fluid Mechanics, Vol. 1* (John Wiley & Sons, New York, 1987), 2nd ed.
 - [18] A. Lindner, J. Vermant, and D. Bonn, Physica A **319**, 125 (2003).
 - [19] H. Chang, E. Demekhin, and E. Kalaidin, Phys. Fluids **11**, 1717 (1999).
 - [20] Y. Amarouchene *et al.*, Phys. Rev. Lett. **86**, 3558 (2001).
 - [21] M. Oliveira and G. McKinley, Phys. Fluids **17**, 071704 (2005).
 - [22] P. Arratia, C. Thomas, J. Diorio, and J. Gollub, Phys. Rev. Lett. **96**, 144502 (2006).
 - [23] G. McKinley and T. Sridhar, Annu. Rev. Fluid Mech. **34**, 375 (2002).
 - [24] F. Trouton, Proc. R. Soc. Lond. A **77**, 426440 (1906).
 - [25] I. Cohen *et al.*, Phys. Rev. Lett. **83**, 1147 (1999).
 - [26] W. Zhang and J. Lister, Phys. Rev. Lett. **83**, 1151 (1999).
 - [27] V. Bergeron *et al.*, Nature **405**, 772 (2000).
 - [28] S. Anna *et al.*, J. Rheol. **45**, 83 (2001).